# Integration of remote sensing and GIS for mapping flash flood hazards, Wadi Queih, Egypt

Asmaa Nasr *, A. Akawy, M. Abdelkareem, and K. Moubark

*Geology Department, Faculty of science, South Valley University, 83523 Qena, Egypt*

## Abstract

Flash floods are common natural events in different environmental conditions. Although, the Egypt's Red Sea area characterized by limited precipitation it frequently impacted by flash flooding. During heavy rainstorms, massive water flow impacting the infrastructures, humans, economic and industrial activities. Thus, the need for mapping vulnerable areas prone to flash flood is necessary. Shuttle Radar Topography Mission data is processed and analyzed to reveal the topographic, geometric, basin relief, texture, and morphometric characteristics for flood risk assessment and mapping of Wadi Queih, in the Red Sea of Egypt. In addition, Tropical Rainfall Measuring Mission (TRMM) data is utilized to display the rainfall zones. The area is classified into eighteen sub-basins. The result revealed that the flash flood potential maps, categorized the sub-basins into five classes, ranging from very low to very high flood potentials and three sub-basins (# 2, 4 and 9) are of extreme hazards. Moreover, the downstream areas are heavily exposed to the risk of flooding. It is noteworthy that storing flood water during rainstorms in artificial depressions will provide more water quantity to support development in remote areas. Additionally, the combination of GIS techniques and remote sensing data allowed for the quick and efficient mapping of flood-prone areas, which assisted decision-makers in reducing the risk of future floods and harvest such water in agricultural activities.

**Keywords:** Flood hazards; GIS; Red Sea; Wadi Queih; Water resources.

## 1. Introduction

Flash floods are one of the major natural threat crises that cause loss and damage of services and infrastructure, human, and economic activities due to an excess of heavy rainfalls that occur quickly and over a short period of time. This is especially true in areas with rugged terrain (Zhang *et al.,* 2015; Elkhrachy, 2015; Abdelkareem, 2017; Zhao *et al.,* 2018; Abdelkareem and Al-Arifi, 2021; Alarifi *et al.,* 2022). Runoff levels have a positive impact on overland flow and speed up its response time. The impact of flash floods in urbanized areas has increased recently because to the unplanned environment, expanding population in emerging nations, and climate change (Bathrellos *et al.,* 2016; Hong and Abdelkareem 2022). Within minutes to a few hours following the start of rainy events, the stream-networks receive substantial water. It involved with too much water in very little time. Thus, in areas of impermeable surface, a cliff, a mountain, and a high topographic relief produces a high runoff. This is because of the climate and topography, controlling flash floods (Abdelkareem, 2017). The fast, quick reaction of a catchment as the level water crests quickly. It takes place in a small, localized basin with varying sizes up to 100 kilometres in length. Consequently, it provided little warning time (Collier, 2007).

Except for sporadic rainfall storms that might result in flash floods, arid regions had dry weather for the whole year. These areas might see more severe fash flood hazard conditions in contrast to other climate regions (Abdelkareem, 2017; Abdel-Fattah, 2017; Abdelkareem and El-Baz, 2015). For leaders to plan for sustaining various activities and prevent flash flood hazards, it is important to identify the areas that are vulnerable to flooding.

Remotely sensed data through GIS techniques are successfully applied in predicting mapping flash flood hazards (Wang *et al.,* 2018; Costache, 2019). By using GIS techniques to analyze remote sensing data, it is possible to compile a variety of datasets, identify high-risk areas, and create maps of flash flood hazards (Abdelkareem, 2017). Therefore, an integrated approach of remote sensing and GIS methodologies will be integrated to assess the hydrologic characteristics and develop a remote sensing-based flash model that utilizes a different set of remote sensing data to identify flood-prone areas and thus assist in flood risk of Wadi Queih area

## 2. Study area

Wadi Queih is a large drainage system that drain to the Red Sea, north of Quseir city that covers approximately 1892.65 km². The wadi drains and cuts through the highly complex terrain that characterizes the Central Eastern Desert and contains several mountains (Figures 1 & 2), G. Abu Zarabit (706m), Umm Khujrah (507m), Duwi (619m), El Hamil (798m), Umm Khalham (886m), Abu Aqarb (773m), El Mour (780m), Mighty Ku (944m), Waira (1037m), El Lubusi (996m) and Semna (1062m). The Red Sea Mountains' tributaries create gorge-like incisions across G. Duwi, with Sodmein Gorge being the most noticeable and well-known for protecting Sodmein Cave.

The mainstream usually flows from west to east and is structurally significantly controlled when it abuts the Queih shear zone. Thus, the branches of W. Queih have distinct directions of Northwest-Southeast, Northeast-Southwest and Southwest. Wadi Queih's lower current also runs mainly along the E-W fault which can run below mean sea level. The mainstream also meanders and turns immediately southward near the el-Saqia area. Wadi el-Saqia runs NW-SE, wadi Semna flows NW-SE, and wadi Sodmein trends NE-SW; these three main tributaries, which correspond to the major faults, split the wadi.

Wadi Queih basin is occupied by Neoproterozoic basement rocks that form part of a horst that is bounded on the east and west by several major normal faults that trend NNW and WNW. The horst is bounded on the west by Cretaceous and Eocene strata of the Duwi structural low, and on the east by Red Sea province Nubia Sandstones and Neogene sediments. The exposed basement rocks are mostly of ophiolitic (serpentinites, basic metavolcanics, and metagabbros), metavolcanics, metasediments, older granites, and Hammamat Groups, which rest unconformably overlying the Dokhan Volcanics in the Wadi Queih basin's northern half. Following Hammamat Groups, the area cut by metagabbro to metadiorites, younger gabbros, younger granites that overlain by Cretaceous/Tertiary succession (Figure 2).

From the north, along the Mediterranean coast, and southward, the amount of precipitation falls, and Cairo only receives a little bit more than one millimetre of precipitation annually. Although there is less intense rainfall in the areas south of Cairo, there might be sudden significant precipitation events that cause flash floods (World Bank Group, 2021). An extremely dry climate with little frequent precipitation characterizes Egypt's Eastern Desert. In the region, precipitation occasionally takes the form of brief yet powerful rainfall episodes. The study area is situated in the arid/hyperarid zone (Figure 3) with an average annual precipitation of roughly 0.0091 to 0.03 mm/day (Figure 3), (January 1998-November 2013), (Abdelkareem and El-Baz, 2015).
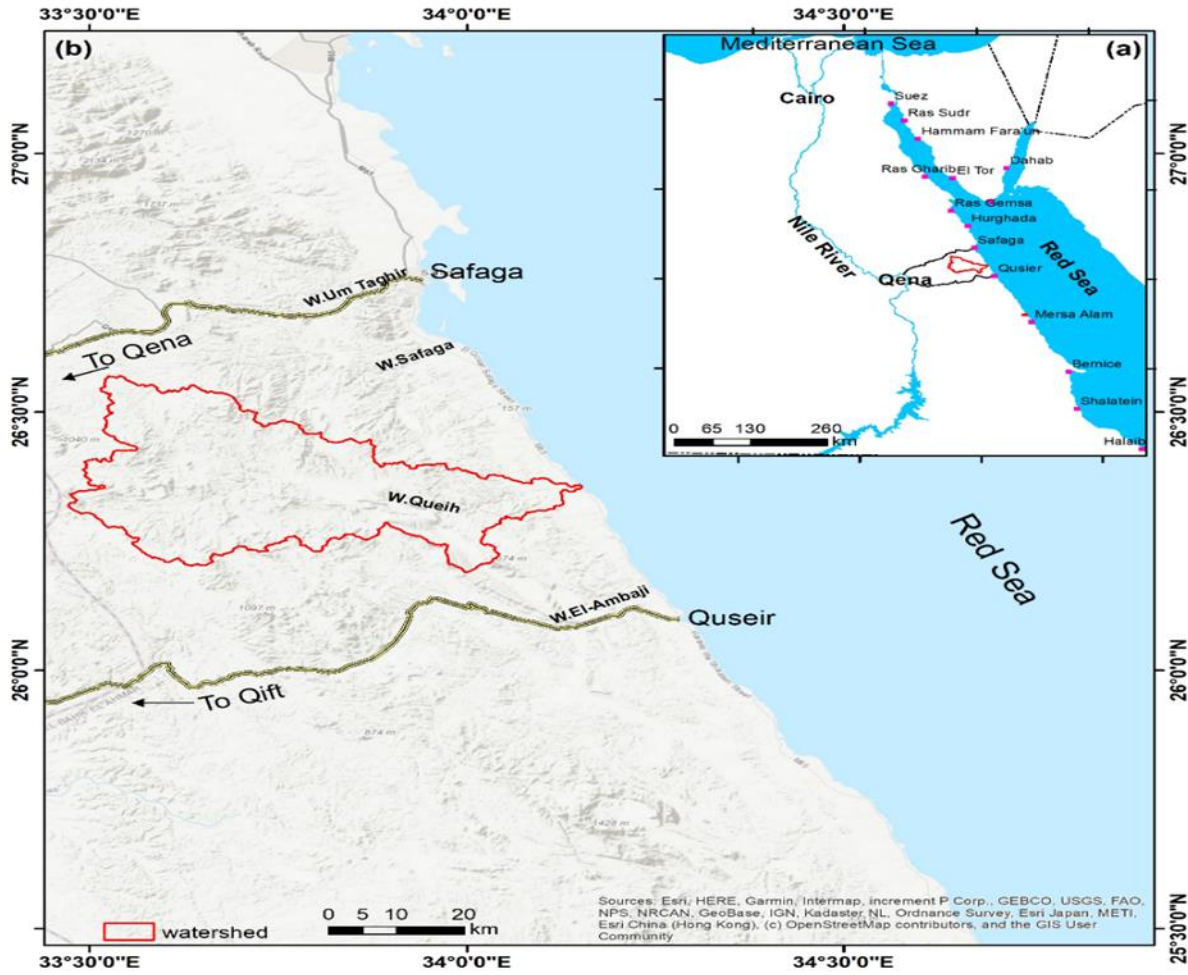
**Figure 1.** Location map of the study area.
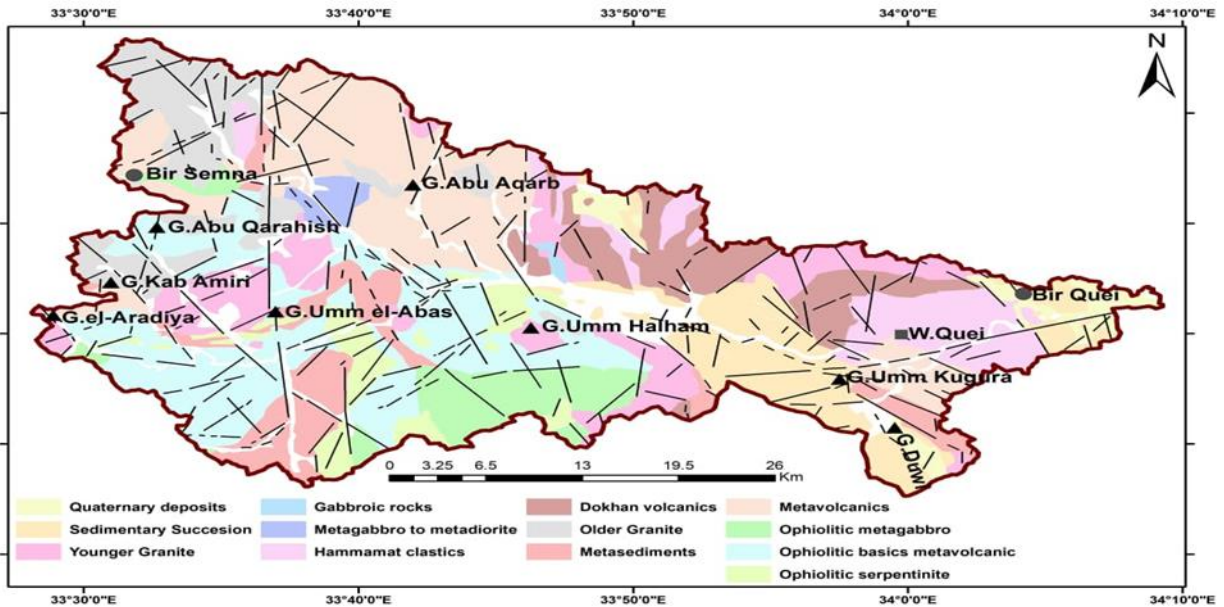


**Figure 2.** Geologic map of the study area (CONOCO, 1987)
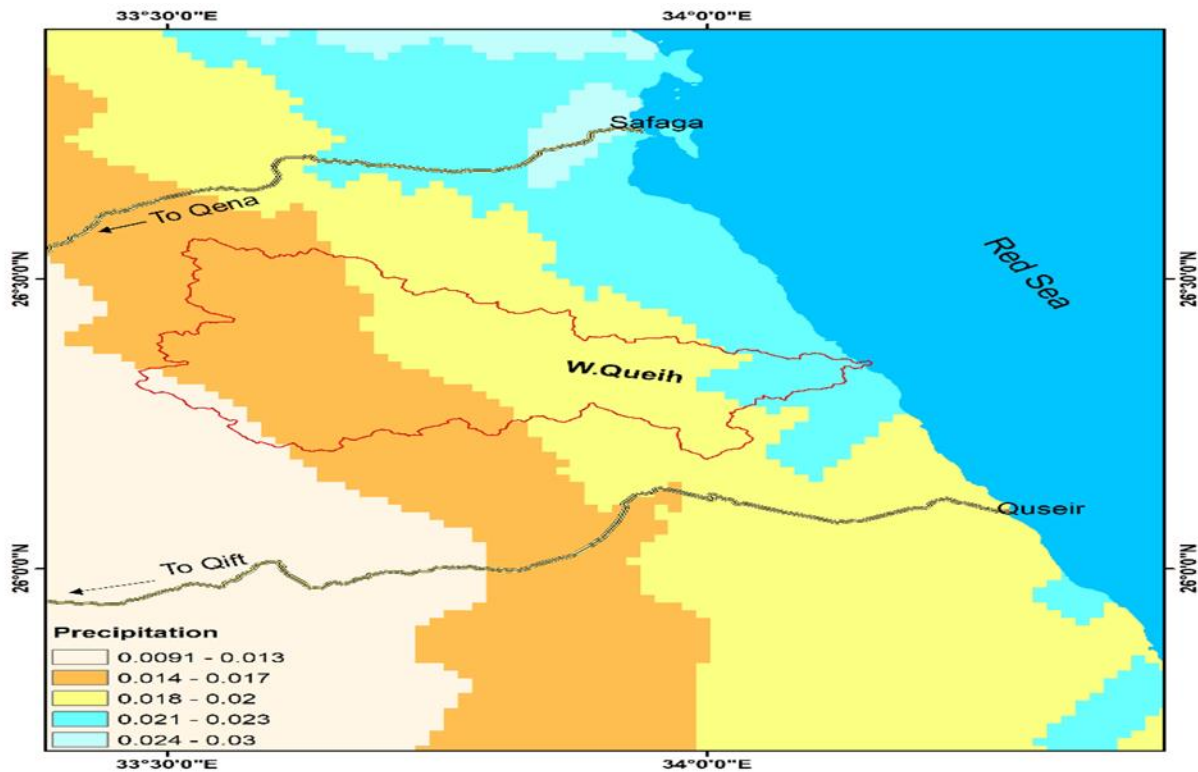
**Figure 3.** Rainfall distribution of the study area

## 3. Data and methods

The SRTM (30 m) data is used to obtain low-elevated sites, slopes, drainages, and altitudes. The eight-deterministic (8-D) technique was used to operate the watershed's regular drainages (O'Callaghan and Mark 1984). Using GIS analysis, the drainage lines were changed to a Dd map. The SRTM DEM can delineate low-elevated extents that serve as sinks, allowing water to reach aquifers in addition to drainage networks (Zhu and Abdelkareem, 2021). The DEM has the ability to quickly and affordably show a watershed's geomorphic and morphometric properties and consent to both qualitative and quantitative explanation (Abdelkareem *et al.,* 2022; Abdelkareem, 2017). The DEM will outline the basin's area (km$^2$), circumference (km), stream order, density, and length ratio.

## 4. Results and discussion

**A**nalysis of topography data in southern Wadi Queih using the SRTM DEM data (Figure 4) revealed that the ground surface elevation ranges from 4 m to 1041 m (above sea level). After employing the surface flow routing algorithm based on the D8 (deterministic eight-node) flow routing algorithm (O'Callaghan and Mark, 1984), the stream network of the research area was recovered using SRTM DEMs data (Figure 5). The sixth order of the stream indicates a matured drainage pattern. The streams display dendritic and rectilinear patterns. Sedimentary rocks which are homogeneous rocks, are reflected in the dendritic shape. The mainstream reaches a length of about 93 km of dendritic to subdendritic drainage patterns modified locally to parallel and less trellis-like patterns, especially in the upstream region (Figure 5).
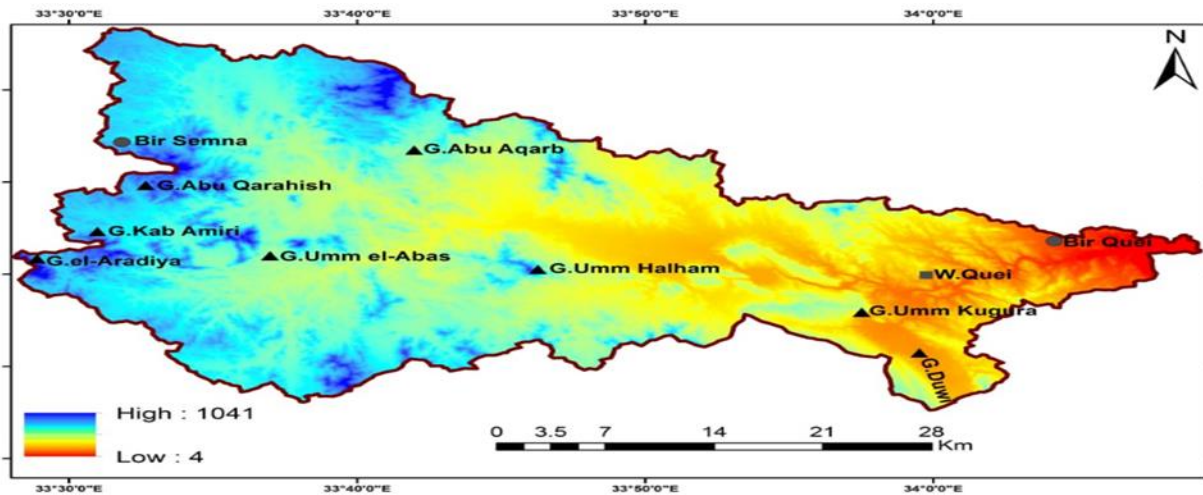
**Figure 4.** The DEM of the W. Queih basin
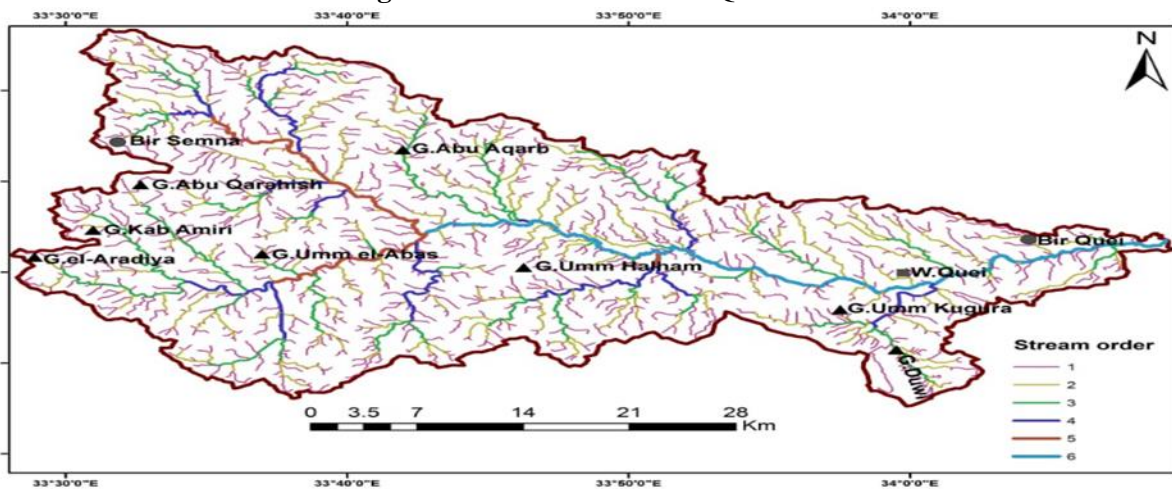


**Figure 5.** stream order of the W. Queih basin

The basin's numerical data was collected by the measurements of remotely sensed data via GIS. Wadi Queih basin has an approximate perimeter (P) of 269 km and an approximate area (A) of 1425 km². The Wadi Queih basin spans 93.6 km from downstream to upstream, or length (Lb). The information that was collected was then used to assess the risk of flash floods, which was determined by the size, shape, relief, and geometry of the basin. Listed in Table 1 are the derived parameters and their formula. WQ is subdivided into 18 sub-basins as shown in (Figure 6). The bifurcation ratio (Rb) of the studied sub-basins ranges from 1.4 to 2.58 with a mean value of 4.295 (Table 1 & Figure 6 a). Concerning the geometric characteristics (Table 1) and shape of

the studied sub-basins, the computed elongation ratio (Re), form factor (Rf), and circularity ratio (Rc) revealed that the basin is not circular in nature but has elongated geometry (Figure 6b, c and d). Re ranges between 0.41 and 0.64, Rf between 0.13 and 0.32, and Rc between 0.12 and 0.34, all of which show an extended shape. This is based on the general classification of elongation ratios into circular (0.9-1.0), oval (0.8-0.9), less elongated (0.7-0.8), elongated (0.5-0.7), and more elongated (0.5) shapes (Schumn, 1956). This is due to form factor values (Rf) being always >0.7584 for a circular basin the values above that are circular geometry (Horton, 1932; Abdelkareem, 2017); however, the present value of Wadi Queih is < 0.75.

**Table 1.** Results of the morphometric parameters of Wadi Queih

| Sub-basin | U-Order | Nu | Lu | Area | Perimeter | Lb | Rb | Re | Rf | Rc | Rt |
|---|---|---|---|---|---|---|---|---|---|---|---|
| 1 | 4 | 99 | 91.28 | 68.94 | 57.92 | 19.33 | 2.43 | 0.48 | 0.18 | 0.26 | 1.71 |
| 2 | 5 | 153 | 135.60 | 105.53 | 70.95 | 21.32 | 2.50 | 0.54 | 0.23 | 0.26 | 2.16 |
| 3 | 5 | 90 | 76.61 | 64.68 | 80.86 | 17.07 | 2.15 | 0.53 | 0.22 | 0.12 | 1.11 |
| 4 | 4 | 83 | 80.30 | 60.74 | 47.36 | 14.43 | 1.56 | 0.61 | 0.29 | 0.34 | 1.75 |
| 5 | 3 | 84 | 65.21 | 54.22 | 64.10 | 20.08 | 2.26 | 0.41 | 0.13 | 0.17 | 1.31 |
| 6 | 5 | 86 | 78.77 | 60.12 | 51.47 | 16.97 | 1.75 | 0.52 | 0.21 | 0.29 | 1.67 |
| 7 | 4 | 31 | 24.88 | 20.80 | 32.76 | 8.84 | 1.56 | 0.58 | 0.27 | 0.24 | 0.95 |
| 8 | 4 | 97 | 90.22 | 67.68 | 63.79 | 19.64 | 2.58 | 0.47 | 0.18 | 0.21 | 1.52 |
| 9 | 5 | 77 | 70.72 | 50.75 | 55.85 | 16.11 | 1.68 | 0.50 | 0.20 | 0.20 | 1.38 |
| 10 | 5 | 141 | 107.78 | 89.99 | 80.31 | 21.98 | 2.13 | 0.49 | 0.19 | 0.18 | 1.76 |
| 11 | 5 | 147 | 153.05 | 120.88 | 81.86 | 29.12 | 1.89 | 0.43 | 0.14 | 0.23 | 1.80 |
| 12 | 5 | 31 | 40.68 | 26.61 | 39.58 | 11.35 | 1.40 | 0.51 | 0.21 | 0.21 | 0.78 |
| 13 | 4 | 103 | 87.02 | 70.43 | 67.15 | 20.59 | 2.36 | 0.46 | 0.17 | 0.20 | 1.53 |
| 14 | 5 | 177 | 163.59 | 130.82 | 84.04 | 21.66 | 1.98 | 0.60 | 0.28 | 0.23 | 2.11 |
| 15 | 5 | 143 | 124.73 | 104.66 | 73.03 | 18.79 | 2.15 | 0.61 | 0.30 | 0.25 | 1.96 |
| 16 | 4 | 71 | 67.17 | 57.38 | 58.16 | 16.48 | 2.06 | 0.52 | 0.21 | 0.21 | 1.22 |
| 17 | 4 | 153 | 124.77 | 97.30 | 76.28 | 18.49 | 2.17 | 0.60 | 0.28 | 0.21 | 2.01 |
| 18 | 4 | 216 | 197.66 | 161.30 | 92.51 | 22.43 | 2.16 | 0.64 | 0.32 | 0.24 | 2.33 |
| Wadi Queih | 6 | 1976 | 1789.18 | 1425.36 | 269.13 | 93.68 | 2.10 | 0.45 | 0.16 | 0.25 | 7.34 |

**Con table 1.** Results of the morphometric parameters of Wadi Queih

| Sub-basin | Fs | Dd | Lg | If | Bh | Rh | Rn | Cm | Basin. W |
|---|---|---|---|---|---|---|---|---|---|
| 1 | 1.44 | 1.32 | 0.38 | 1.90 | 0.54 | 0.03 | 0.72 | 0.76 | 11.56 |
| 2 | 1.45 | 1.28 | 0.39 | 1.86 | 0.58 | 0.03 | 0.75 | 0.78 | 7.96 |
| 3 | 1.39 | 1.18 | 0.42 | 1.65 | 0.53 | 0.03 | 0.63 | 0.84 | 7.03 |
| 4 | 1.37 | 1.32 | 0.38 | 1.81 | 0.60 | 0.04 | 0.80 | 0.76 | 10.81 |
| 5 | 1.55 | 1.20 | 0.42 | 1.86 | 0.70 | 0.03 | 0.84 | 0.83 | 4.75 |
| 6 | 1.43 | 1.31 | 0.38 | 1.87 | 0.56 | 0.03 | 0.74 | 0.76 | 7.26 |
| 7 | 1.49 | 1.20 | 0.42 | 1.78 | 0.37 | 0.04 | 0.44 | 0.84 | 6.73 |
| 8 | 1.43 | 1.33 | 0.38 | 1.91 | 0.59 | 0.03 | 0.79 | 0.75 | 6.68 |
| 9 | 1.52 | 1.39 | 0.36 | 2.11 | 0.61 | 0.04 | 0.85 | 0.72 | 5.49 |
| 10 | 1.57 | 1.20 | 0.42 | 1.88 | 0.54 | 0.02 | 0.65 | 0.83 | 10.33 |
| 11 | 1.22 | 1.27 | 0.39 | 1.54 | 0.68 | 0.02 | 0.86 | 0.79 | 9.74 |
| 12 | 1.17 | 1.53 | 0.33 | 1.78 | 0.37 | 0.03 | 0.56 | 0.65 | 3.83 |
| 13 | 1.46 | 1.24 | 0.40 | 1.81 | 0.49 | 0.02 | 0.60 | 0.81 | 5.16 |
| 14 | 1.35 | 1.25 | 0.40 | 1.69 | 0.61 | 0.03 | 0.76 | 0.80 | 10.71 |
| 15 | 1.37 | 1.19 | 0.42 | 1.63 | 0.57 | 0.03 | 0.68 | 0.84 | 7.53 |
| 16 | 1.24 | 1.17 | 0.43 | 1.45 | 0.50 | 0.03 | 0.59 | 0.85 | 7.36 |
| 17 | 1.57 | 1.28 | 0.39 | 2.02 | 0.49 | 0.03 | 0.62 | 0.78 | 8.55 |
| 18 | 1.34 | 1.23 | 0.41 | 1.64 | 0.54 | 0.02 | 0.66 | 0.82 | 12.59 |
| Wadi Queih | 1.39 | 1.26 | 0.40 | 1.74 | 1.04 | 0.01 | 1.30 | 0.80 | 24.69 |

Based on Smith (1950) classification (i.e., very coarse < 2, coarse 2–4, moderate 4–6, fine 6–8, and very fine >8), the present study drainage texture (Figure 6e) which ranges from 0.78 to 2.33, for the studied sub-basins seems to be a moderate drainage texture. Furthermore, the stream frequency (Fs) of the studied sub-basins ranges from 1.16 to 1.57 (Figure 6 f) revealing that the drainage controlled by the basin lithology (Kale and Guptha, 2001). Additionally, the drainage density (Dd) of areas between streams has an impact on the runoff that accumulates over time, and a higher value accelerates the runoff. Density in the Wadi Queih drainage ranges between 1.17 and 1.53 km/km$^2$. Furthermore, the length of overland flow (Lg), which ranges from

0.33 to 0.43 and shows that surface water runoff accumulates more quickly than values with high values (Figure 3h), indicates a significant hazard. The infiltration number (lf; Faniran 1968) is obtained by multiplying the Fs by the Dd. The range of the sub-basins under study is 1.45 to 2.11. The much higher values demonstrate greater runoff and less infiltration ability (Figure 6 i). The altitude variation in between maximum height (Z) of the watershed and the lowest point (z) on the valley floor is referred to as the basin relief (Bh) (Strahler, 1957). Therefore, the Bh values in the Wadi Queih sub-basins range from 0.37 (sub-basins 5 and 11) to 0.70 km (sub-basins 7 and 12) (Figure 6 j). High runoff and a greater flood peak are indicated by a higher value for Bh.
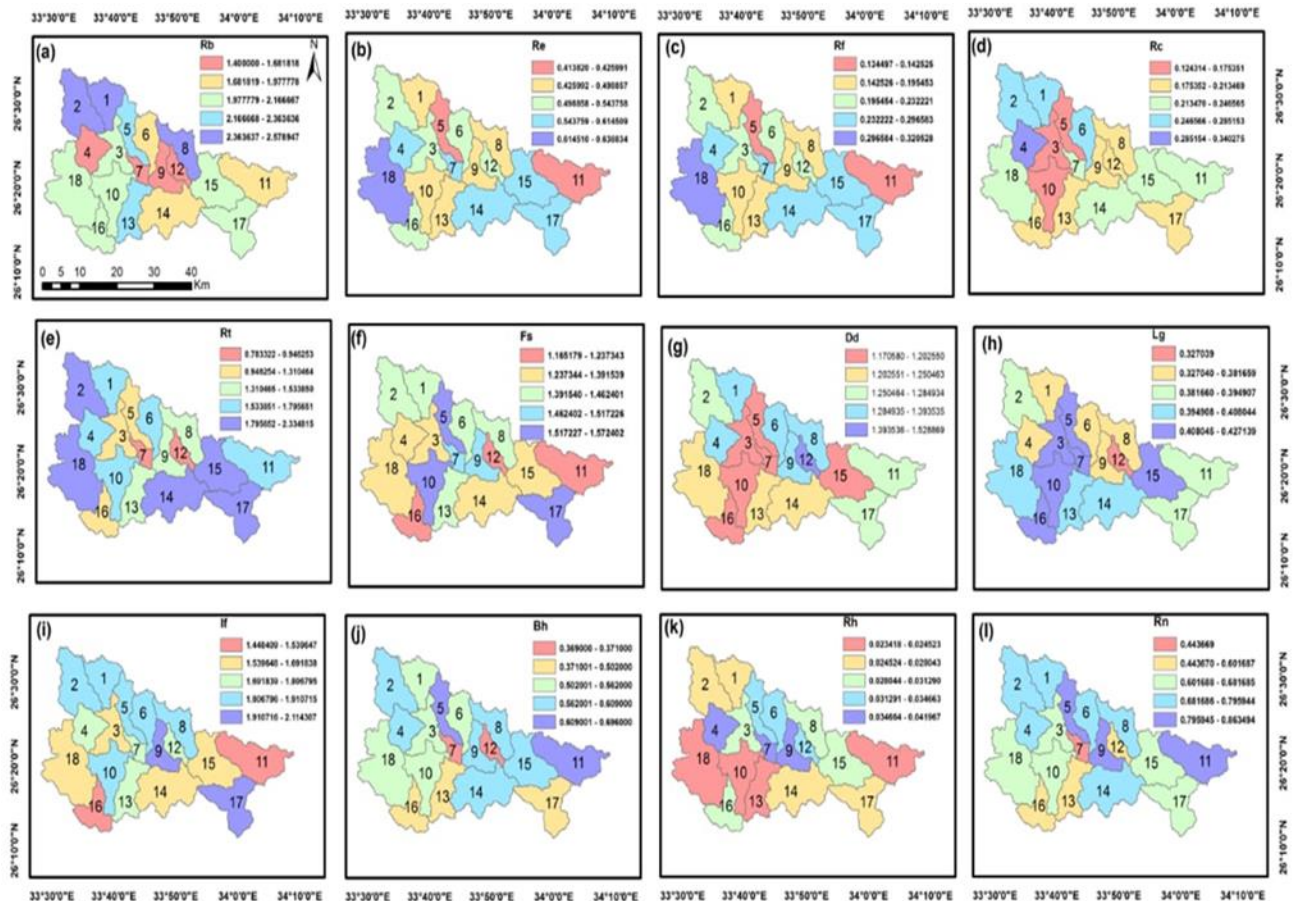


**Figure 6.** Morphometric parameters of W. Queih (a) Bifurcation ratio (Rb); (b) elongation ratio (Re); (c) form factor (Rf); (d) circularity ratio (Rc); (e) texture ratio (T); (f) stream frequency (fs); (g) drainage density (Dd); (h) length of overland flow (lg); (i) infiltration number (if); (k) basin relief (Bh); (m) relief ratio (Rh); (n) ruggedness number (Rn).

By dividing Bh by the longest possible basin length (Lb), which yields a dimensionless ratio, one can get the Relief ratio Rh (Schumm, 1956). Additionally, it serves as a gauge for a river basin's overall steepness and as a gauge for how vigorously the erosion process is taking place on the basin's slope. Wadi Queih sub-basin's Rh values range from 0.02 to 0.04 km (Figure 6 k). Higher numbers show higher runoff and high-risk zones. Because of the steep terrain connecting the sub-basins 10, 11, 13, and 18, which exhibit higher value. Additionally, the Ruggedness number can be computed by multiplying maximum basin relief (Bh) and drainage density (Dd). A higher value represents steep slope (Strahler 1957; 1964). The results of Rn values range from 0.44 to 0.86.  Higher values reveal

higher relief and runoff such as sub-basins 5, 9, and 11 (Figure 6 l).

Many techniques, including statistical and qualitative characterization, have been used to create flash flood mapping (Abdelkareem, 2017). The flash flood hazard map in this study was calculated using the following two methods. Integrated raster maps of a few morphometric parameters, and the Davis (1975) linear equations (Abdelkareem, 2017).

To map the possible locations of a flash flood, numerous morphometric parameters of GIS layers were combined using the GIS overlay approach (Figure 7 a). There are various parameters that displayed in Table 1 (Figure 7) beyond a certain threshold promote runoff and increase the peak of a flood (Abdelkareem, 2017).
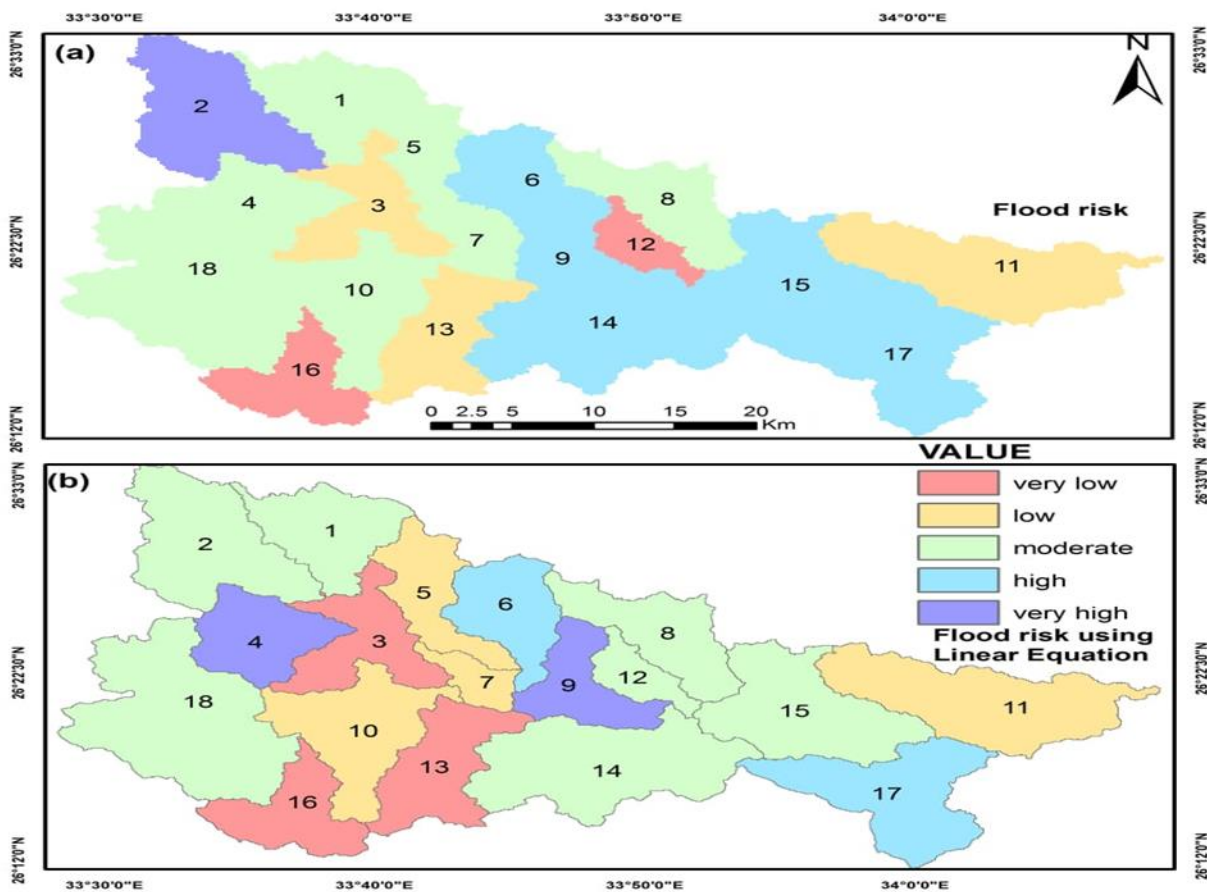


**Figure 7.** Flood potential maps a flood potential map based on integrated thematic layers, b flood potential map based on linear equation (Davis, 1975)

Additionally, the greater values of T, Fs, Dd, and If reflect the abundance of the streams per area and perimeter, which higher runoff. The circular sub-basins, not the elongated ones, were shown by the greater values of Re, Rf, and Rc (Abdelkareem, 2017). This is due to the runoff's quick transit time rather than the long travel time of elongated sub-basins. exhibited higher values of Bh, Rh, and Rn. The flood potential map categorized the sub-basins into 5 groups (Table1) based on the combined morphometric characteristics (Figure 7 a), including very low, low, moderate, high and very high; the very low includes sub-basins 12, and 16 but extremely high includes sub-basin 2.

Numerous morphometric parameters, including Re, Rf, Rc, T, Fs, Dd, If, Bh, Rh, and Rn (Table 1), which have a favorable association with the runoff and flood potential, were estimated using a linear equation (Davis, 1975). The bifurcation ratio (Rb) and length of overland flow (Lg), however, were also computed because they have adverse correlations. All variables have been given a risk scale number, ranging from 1 (lowest) to 5 (highest). Based on this approach, sub-basins 4 and 9 revealing high flooding risk (Figure 7 b).

## 5. Conclusions

Wadi Queih, in the Red Sea of Egypt was studied using remote sensing and GIS analysis to reveal the potential areas of flash flood hazards using two different statistical and geospatial approaches. To do this, the topography, geometric, basin relief, texture, and morphometric properties for flood risk assessment and mapping are revealed through the processing and analysis of data from the SRTM DEM with the aid of rainfall data derived from TRMM data. A total of eighteen sub-basins make up the area. The outcome showed that the sub-basins were divided into five classes according to their flash flood potential, ranging from very low to very high flood potentials, and that three of them (sub-basins #2, #4, and 9) are particularly

dangerous. Additionally, there is a significant risk of flooding in the downstream areas. Notably, artificial reservoirs can have the capability to catch flood water during rainstorms will increase the amount of water available to support development in outlying areas. Additionally, the use of remote sensing data in conjunction with GIS techniques made it possible to quickly and effectively map areas that were vulnerable to flooding, helping decision-makers lower the likelihood of future floods.

## 6. References

Abdel-Fattah M., Saber M., Kantoush S., Khalil M., Sumi T., Sefelnasr A. A. (2017). 'Hydrological and Geomorphometric Approach to Understanding the Generation of Wadi Flash Floods', *Water,* 9(7), pp. 553.

Abdelkareem M., El-Baz, F. (2015). 'Analyses of optical images and radar data reveal structural features and predict groundwater accumulations in the central Eastern Desert of Egypt', *Arab J. Geo. sci.,* 8, pp. 2653–2666.

Abdelkareem, M. (2017). 'Targeting flash flood potential areas using remotely sensed data and GIS techniques', *Nat. Hazards J.,* 85, pp. 19–37.

Abdelkareem, M., Al-Arifi, N., Abdalla, F., Mansour, A., El-Baz, F. (2022). 'Fusion of Remote Sensing Data Using GIS-Based AHP-Weighted Overlay Techniques for Groundwater Sustainability in Arid Regions', *Sustainability,* 14, 7871.

Alarifi, S.S., Abdekareem, M., Abdalla, F., Alotaibi, M. (2022). 'Mapping Susceptible Areas to Flash Flood Hazards Using Remote Sensing and GIS Techniques in the Southwest Part of Saudi Arabia', *Sustainability,* 14, x. https://doi.org/10.3390/xxxxx

Bathrellos, G.D., Karymbalis, E., Skilodimou, H.D., Gaki-Papanastassiou, K., Baltas, E.A. (2016). 'Urban flood hazard assessment in the basin of Athens Metropolitan city, Greece', *Environ. Earth Sci.*, 75, 319.

Collier, C.G. (2007). 'Flash flood forecasting: What are the limits of predictability?', *Q. J. Meteorol. Soc.,* 133.

Costache, R. (2019). 'Flash-flood potential index mapping using weights of evidence, decision trees models and their novel hybrid integration', *Stoch. Environ. Res. Risk Assess.,* 33, pp. 1375–1402.

Davis, J.C. (1975). *'Statics and data analysis in geology',* Wiley, New York

Hong, Y., Abdelkareem, M. (2022). 'Integration of remote sensing and a GIS-based method for revealing prone areas to flood hazards and predicting optimum areas of groundwater resources', *Arab. J. Geo. sci.,* 15, pp. 1–14.

Wang, Y., Hong, H., Chen, W., Li, S., Pamucar, D., Gigovic, L., Drobnjak, S., Tien Bui, D., Duan, H. A. (2018). 'hybrid GIS multi-criteria decision-making method for flood susceptibility mapping at Shangyou, China', *Remote Sens.,* 11, 62.

World Bank Group. (2021). *'Climate risk country profile: EGYPT',* 23 p. https://climateknowledgeportal.worldbank.org (accessed on 6 September 6, 2022)

Zhang D., Quan J., Zhang H. (2015). 'Flash flood hazard mapping: A pilot case study in Xiapu River Basin, China', *Water Science and Engineering,* 8(3), 195e204.

Zhao, G., Pang, B., Xu, Z., Yue, J., Tu, T. (2018). 'Mapping flood susceptibility in mountainous areas on a national scale in China', *Sci. Total Environ.,* 615, pp. 1133–1142.

Zhu, Q., Abdelkareem, M. (2021). 'Mapping groundwater potential zones using a knowledge-driven approach and GIS analysis', *Water,* 13, pp. 579.